Comparative study on the ionic conductivities and redox properties of $LiPF_6$ and LiTFSI electrolytes and the characteristics of their rechargeable lithium ion batteries

A R Septiana[1], W Honggowiranto[2], Sudaryanto[2], E Kartini[2,a], R Hidayat[1,b]

[1] Physics Program Study, Faculty of Mathematics and Natural Sciences, Institut Teknologi Bandung, Jl. Ganesha 10, 40132, West Java, Indonesia
[2] Center for Science and Technology of Advanced Material, National Nuclear Energy Agency of Indonesia, Kawasan PUSPIPTEK Serpong, Tangerang Selatan, 15314, Banten, Indonesia

[a]kartini@batan.go.id
[b]rahmat@fi.itb.ac.id

Abstract. The ionic conductivities of two different electrolytes, namely lithium hexafluorophosphate ($LiPF_6$) and lithium bis (trifluoromethylsulfonyl) imide (LiTFSI), in carbonate-based solvents have been investigated. The ionic conductivity of LiTFSI electrolyte is slightly larger than the $LiPF_6$ electrolyte, namely 2.7 mS/cm *vs*. 2.4 mS/cm. The results of cyclic voltammetry and electrochemical impedance spectroscopy measurements show that LiTFSI electrolyte exhibit a better reversible redox reaction. Therefore, in this work, the full-cell battery using LiTFSI electrolyte exhibited higher specific capacity than the battery cell using $LiPF_6$ electrolyte, namely 83.1 mAh/g and 101.5 mAh/g for the $LiPF_6$ and LiTFSI electrolytes, respectively. Higher capacity in LiTFSI battery is thus related to better ionic conductivity and reversible redox reaction of LiTFSI electrolyte.

1. Introduction

For more than two decades, lithium-ion batteries (LIBs) have become an important energy storage for portable electronics, such as mobile phones, communication devices, laptops, digital audio players etc. Currently, LIBs have been also developed as high-power electric storages for renewable energy and electric vehicles applications due to its superior performance, flexibility in design, high energy, and excellent power density properties [1–3]. However, such applications require more chemically and thermally stable electrolytes, where the electrolyte composition plays an important role. The electrolytes used in LIB are commonly comprised of a lithium salt, a mixture of organic solvents and additives [4]. Commercially available LIB mostly contain lithium hexafluorophosphate ($LiPF_6$) in mixtures of organic carbonate solvents as the electrolyte due to its high conductivity [5–10]. However, $LiPF_6$ is thermally unstable and may decompose to LiF and PF_5. Moreover, PF_5 is highly reactive to water and hydrolize to form HF and PF_3O, where HF is highly reactive acid and corrosive. It may attack both negative and

positive electrodes, resulting in the battery performance reduction [11, 12]. The detailed mechanism of reaction between water and $LiPF_6$ in organic solvents has been reported in previous research [10, 12, 13]. Due to this drawback, the use of other lithium salts should also be seriously considered [8, 9, 14, 15]. Among some alternatives, lithium bis(trifluoromethylsulfonyl) imide (LiTFSI) have been considered as one of promising alternative because of less moisture reactivity, better ionic dissociation, high thermal and high electrochemical stability in comparison to $LiPF_6$ [16, 17].

In this paper, we reported the results of our comparative study on LiTFSI and $LiPF_6$ electrolytes on their ionic conductivity and their electrochemical properties as well as the charge-discharge capacity of LIB using these electrolytes.

2. Experimental

In this research, 1M LiTFSI in EC:DEC (1:1) and 1M $LiPF_6$ in EC:DEC (1:1) solutions were used as the electrolytes, where EC is ethylene carbonate and DEC is diethylene carbonate. The solutions were prepared in a glove box filled with an inert gas atmosphere. The ionic conductivity of LiTFSI and $LiPF_6$ electrolytes were determined from the results of the Electrochemical Impedance Spectroscopy (EIS) measurements, using a Hioki 3532-50 LCR Hi-Tester with the frequency range of 42 Hz up to 1 MHz. The electrolyte was put inside a CR2016 coin-type cell in between of a pair of two stainless steel electrodes (stainless steel | electrolyte | stainless steel). With known cell dimensions, the conductivity σ can be obtained from the following formula [18]:

$$\sigma = \frac{t}{A}\frac{1}{R_b} \tag{1}$$

where t is the thickness of the electrolyte layer (cm), A is the effective contact area (cm^2) and R_b is the bulk resistance (Ω).

For the cyclic voltammetry (CV) measurements, the coin cell used for the measurement consists of a lithium metal as an anode and $LiFePO_4$ as a cathode. The cell was swept at 50μV/s scan rate and voltage range of 2-4 V. For the charge-discharge characterizations, the coin cells were consisting of a graphite as the negative electrode and $LiFePO_4$ as the positive electrode, which was separated by a polypropylene microporous separator (celgard). The electrodes were heated at 80°C under vacuum for 12h before assembled. The charge-discharge characterizations were conducted using an 8-Channel Battery Analyzer at 0.1 C rate.

3. Results and discussions

3.1. Electrolyte conductivity

The conductivity of the electrolyte plays a key role because the internal resistance of the battery cell is mostly due to the electrical resistivity of the electrolyte solution [19]. The measured frequency-dependent ionic conductivity of these electrolytes are shown in Figure 1. As shown in this figure, the ionic conductivity spectra consist of two regions in the frequency range, where at the low-frequency dispersive region is due to the electrode polarization effects and the frequency independent plateau region corresponds to the dc conductivity of the electrolyte. This is a typical characteristic of Li salt electrolytes as reported elsewhere [20]. The ionic conductivities were then calculated using equation (1), where the R_b values were taken from their plateau region, resulting in the ionic conductivity values of 2.7 mS/cm and 2.4 mS/cm for LiTFSI and $LiPF_6$ electrolytes, respectively. The measured ionic conductivities of these salts here are slightly lower than for the result as reported by Murmann *et al*., which may be affected by the presence of membrane separator used in the cells here [21].

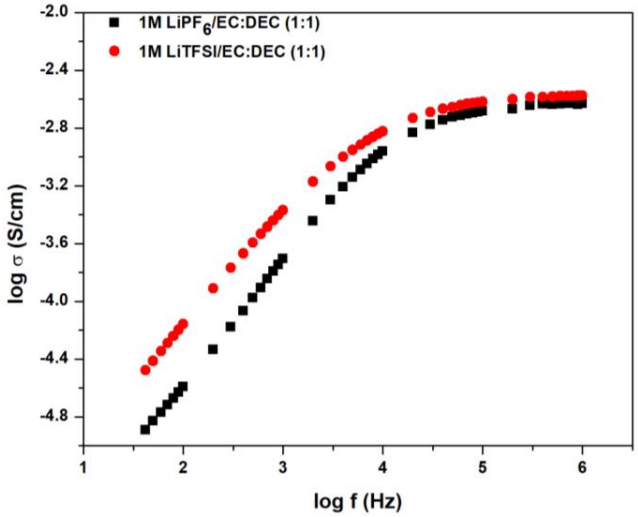

Figure 1. The frequency-dependent ionic conductivity spectra of the LiTFSI and $LiPF_6$ electrolytes.

3.2. Cyclic voltammetry characteristics

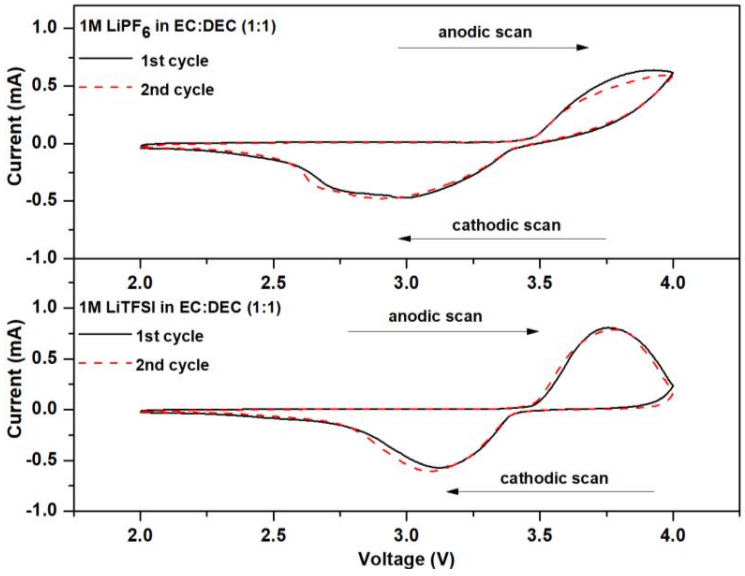

Figure 2. The CV curves of the Li/$LiFePO_4$ full cell batteries with different electrolytes, namely $LiPF_6$ and LiTFSI, taken at 50μV/s scan rate.

Figure 2 shows the CV curves of the Li/$LiFePO_4$ full cell batteries using LiTFSI and $LiPF_6$ electrolytes. For the $LiPF_6$ electrolyte, the redox peaks can be clearly seen at around 3 V and 3.9 V *vs*. Li/Li^+. For the LiTFSI electrolyte, the redox peaks are at around 3.1 V and 3.75 V vs. Li/Li^+. For a comparison, Wang *et*

al. reported that the oxidation and reduction peaks for a Li/$LiFePO_4$ cells are at about 3.6 V and 3.3 V [22]. In general, CV shape with more symmetry and narrower redox peaks would indicate a better electrochemical activity. The figure thus indicates that the cell using LiTFSI electrolyte shows a better electrochemical activity in comparison to that using $LiPF_6$ electrolyte. Moreover, the areas of the oxidation and reduction peaks for the battery using LiTFSI electrolyte are almost the same, indicating highly reversible redox reaction. However, the battery using $LiPF_6$ based electrolyte show unequal oxidation and reduction peaks, indicating less reversible redox reaction. The midpoint of the anodic and cathodic peaks is about 3.425 V for the cell using LiTFSI electrolyte and 3.450 V for the cell using $LiPF_6$ electrolyte, which corresponds to the open-circuit voltage (OCV) of the battery [23].

3.3. Charge-discharge and EIS characteristics

The electrochemical process on the electrodes during charging process is:

Cathode : $LiFePO_4 \rightarrow FePO_4 + Li^+ + e^-$ [24]

Anode : $Li^+ + e^- \rightarrow Li$

The electrochemical process on the electrodes during discharging process is:

Cathode : $FePO_4 + Li^+ + e^- \rightarrow LiFePO_4$

Anode : $Li \rightarrow Li^+ + e^-$

Figure 3 shows the measured charge-discharge curves of these batteries taken at the charge-discharge rate of 0.1 C. Shown in the figure is the first cycle and the fifth cycle only, drawn in the voltage range of 2.5-3.8V for their vertical axis. It can be seen that there is a plateau region with the potential at around 3.3-3.4 V. The specific charge and discharge capacity at the first cycle for the battery using $LiPF_6$ electrolyte is 89.7 mAh/g and 83.1 mAh/g, while it is larger, namely 105.7 mAh/g and 101.5 mAh/g, for the battery using LiTFSI electrolyte. Capacity loss upon the first cycle is mainly due to the loss of lithium resulting from the formation of the Solid Electrolyte Interphase (SEI) at the surface of the graphite negative electrode as reported by Castro *et al*. [24]. The charge and discharge capacity seems to decrease slightly with the number of cycles.

In order to understand the observed difference in their charge-discharge capacity, the EIS measurements have also been carried out after the first and fifth cycles. EIS is a versatile tool for investigating the impedance changes due to characteristics changes in the electrodes and electrolyte caused by any irreversible or undesired reactions inside the cell, such as excessive SEI formation [25, 26].

Figure 4 shows the Nyquist plots obtained from the EIS measurements of these battery cells at a dc bias voltage of 0V taken after the first and fifth charge-discharge cycles. It seems that the shape of those Nyquist plots for both batteries are almost similar. However, it can be clearly seen that the semicircle for the cell using $LiPF_6$ electrolyte becomes much larger after the fifth charge-discharge cycle. This may indicate the increase in the resistance or/and the decrease in capacitance. In general, the semicircle part at the high-middle frequency region may correspond to the charge transfer resistance (R_{ct}). The inclined line at the low-frequency region may be related to the Warburg impedance (W), that reflects the diffusion of Li^+ in the active material [26, 27].

In order to better understand on the difference in their impedance characteristics, those Nyquist plots were fitted by an equivalent circuit as shown in Figure 4 [28–31]. The equivalent circuit consists of a resistor (R_1) describing the bulk resistance of the cell and two R|CPE elements connected in series. The first RC element (R_2 in parallel with CPE_1) is related to various layers formed as the electrode surface (SEI formation). The constant phase element (CPE) is related to the non-ideal capacitor behavior, which is quantified by the n value in between 0 and 1. If n is equal to 1, the CPE then behaves as an ideal capacitor.

A non-ideal capacitor behavior may arise from the presence of SEI layer. The second RC element is attributed to the interfacial processes (charge transfer) controlled by the lithium ion diffusion into graphite,

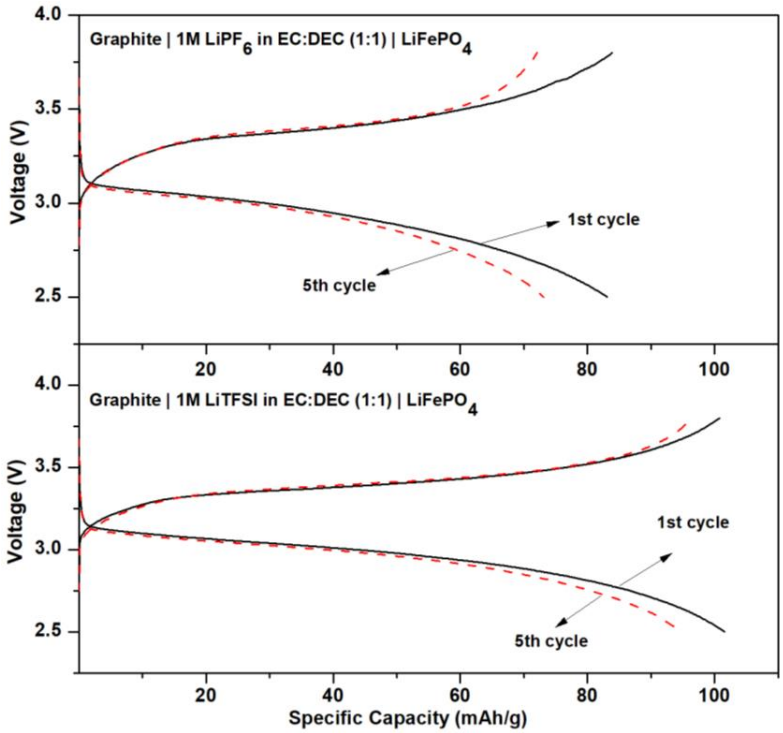

Figure 3. Charge-discharge curves of full-cell (Graphite |electrolyte |$LiFePO_4$) batteries using $LiPF_6$ and LiTFSI electrolytes taken at 0.1 C rate.

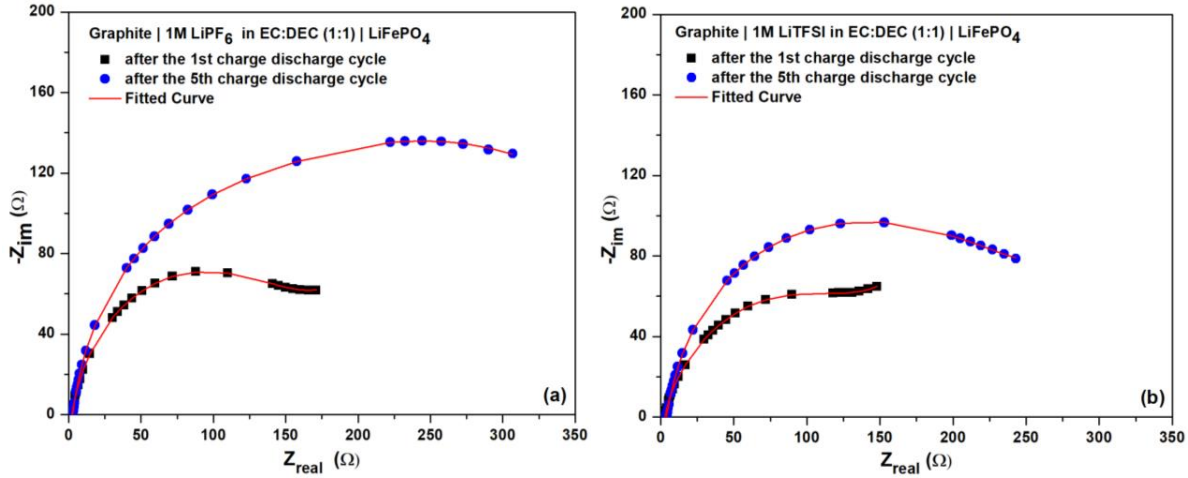

Figure 4. The Nyquist plots obtained from the EIS measurements of the (Graphite |electrolyte |$LiFePO_4$) battery cells using $LiPF_6$ and LiTFSI electrolytes taken after the first and fifth charge-discharge cycles. The thin lines represent the fitting curves.

which is modeled with a Warburg impedance [32]. The combination of R_3 and *Zw* is commonly called as the Faradic impedance. Low R_3 value generally corresponds to a fast kinetics of the faradic reaction [28].

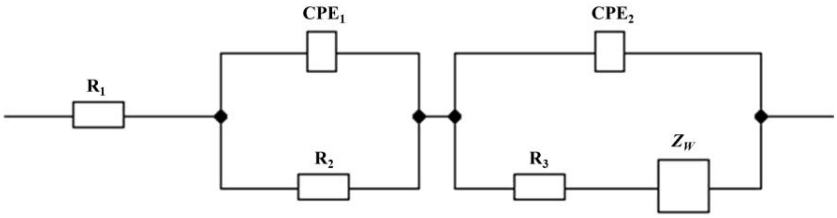

Figure 5. The equivalent circuit used in the curve fitting of the Nyquist plots in Figure 4.

Table 1. The obtained fitting parameters of the equivalent circuit model for the Nyquist plots in Figure 4.

Parameter	1M $LiPF_6$ in EC:DEC (1:1)		1M LiTFSI in EC:DEC (1:1)	
	1st cycle	5th cycle	1st cycle	5th cycle
R_1 (Ω)	2.27	2.83	2.90	3.94
R_2 (Ω)	122.17	253.73	108.44	162.25
R_3 (Ω)	33.63	120.10	8.71	73.93
Aw ($\Omega s^{0.5}$)	584.40	439.52	734.30	562.88
CPE_1 (μF)	17.241	28.561	21.824	23.201
n_1	0.722	0.811	0.809	0.788
CPE_2 (μF)	6.312	3.739	5.880	3.658
n_2	0.912	0.955	1.000	0.987

The fitting results are tabulated in Table 1. Based on these fitting results, taken after the fifth charge-discharge cycle, the first RC element (R_2|CPE_1) of the cells slightly change. However, the cell using LiTFSI electrolyte shows a much smaller increase in its R_2 and CPE_1 values in comparison to the cell using $LiPF_6$ electrolyte. This may indicate less continues SEI layer formation in the cell using LiTFSI. This is in agreement with a smaller capacity reduction in the fifth charge-discharge cycles for the cell using LiTFSI electrolyte. In addition, for the second RC element, the higher R_3 values in the cell using $LiPF_6$ electrolyte may indicate a slower kinetics of redox reaction and it thus leads to a smaller battery capacity. This is consistent with the observed charge-discharge capacity above, where the cell using $LiPF_6$ electrolyte shows a smaller battery capacity in comparison to the cell using LiTFSI electrolyte.

4. Conclusion

LiTFSI in EC:DEC electrolyte shows a slightly larger ionic conductivity in comparison to $LiPF_6$ in EC:DEC electrolyte. In addition, the LiTFSI electrolyte also shows a more reversible cyclic voltammetry shape, indicating more reversible redox of Li^+ ions in the battery. The charge-discharge capacity of the battery cell using LiTFSI electrolyte also show higher capacity and smaller increasing with number of cycles. Therefore, these experimental results show that the LiTFSI electrolyte has more superior characteristics compared to the $LiPF_6$ electrolyte.

Acknowledgments

This work was partly supported by Program Molina, LPDP – ITB and partly supported by Program INSINAS Riset PRATAMA Konsorsium 2016.

References

[1] Ryou M Lee J Lee D Kim W Jeong W K Choi J W Park J Lee Y M 2012 *Electrochim Acta* **83** 259–63
[2] Alias N and Mohamad AA 2015 *J. Power Sources* **274** 237–51
[3] Zhang R Chen Y and Montazami R 2015 *Materials* **8** 2735–48
[4] Zhang B Zhou Y Li X Ren X Nian H Shen Y Yun Q 2013 *Int. J. Electrochem. Sci.* **8** 12735–40
[5] Yang H and Zhuang G Jr PR 2006 *J. Power Sources* **161** 573–9
[6] Gnanaraj JS Thompson RW Dicarlo JF and Abraham KM 2007 *J. Electrochem. Soc.* **154** A185–91
[7] Zhang Z Chen X Li F Lai Y Li J Liu P Wang X 2010 *J. Power Sources* **195** 7397–402
[8] Dougassa YR Tessier C El-Ouatani L Anouti M Jacquemin J 2013 *J. Chem. Thermodyn.* **61** 32–44
[9] Zhang L Chai L Zhang L Shen M Zhang X Battaglia VS Stephenson T Zheng H 2014 *Electrochim. Acta* **127** 39–44
[10] Kawamura T Okada S and Yamaki J 2006 *J. Power Sources* **156** 547–54
[11] Chen Z Lu WQ Liu J and Amine K 2006 *Electrochim. Acta* **51** 3322–6
[12] Lux SF Lucas IT Pollak E Passerini S Winter M Kostecki R 2012 *Electrochem. Commun.* **14** 47–50
[13] Sloop SE Pugh JK Wang S Kerr JB Kinoshita K 2001 *Electrochem. Solid-State Lett.* **4** A42–4
[14] Zhang SS Xu K and Jow TR 2006 *J. Power Sources* **156** 629–33
[15] Shieh DT Hsieh PH and Yang MH 2007 *J. Power Sources* **174** 663–7
[16] Bolloli M Alloin F Kalhoff J Bresser D Passerini S Judeinstein Lepretre JC Sanchez JY 2015 *Electrochim. Acta* **161** 159–70
[17] Yang B Li C Zhou J Liu J Zhang Q 2014 *Electrochim. Acta* **148** 39–45
[18] Osman Z Mohd Ghazali MI Othman L Md and Isa KB 2012 *Results Phys*. **2** 1–4
[19] Dahbi M Ghamouss F Tran-Van F Lemordlant D Anouti M 2011 *J. Power Sources* **196** 9743–50
[20] Vijaya N Selvasekarapandian S Malathi J Iwai Y Nithya H Kawamura J 2012 *Proc. of the 13th Asian Conf. on Solid State Ionics* 342–33
[21] Murmann P Niehoff P Schmitz R Nowak S Gores H Ignatiev N Sartori P Winter M Schmitz R 2013 *Electrochim. Acta* **114** 658–66
[22] Wang WL Jin EM and Gu H-B 2012 *Trans. Electr. Electron. Mater.* **13** 121–4
[23] Yu DYW Fietzek C Weydanz W Donoue K Inoue T Kurokawa H Fujitani S 2007 *J. Electrochem. Soc.* **154** A253–7
[24] Castro L Dedryvère R Ledeuil J-B Breger J Tessier C Gonbeau D 2012 *J. Electrochem. Soc.* **159** A357–63
[25] Aurbach D 2000 *J. Power Sources* **89** 206–18
[26] Gao P Zhang C and Wen G 2015 *J. Power Sources* **294** 67–74
[27] Wang L Zhao J He X Gao J Li J Chunrong W and Changyin J 2012 *Int. J. Electrochem. Sci.* **7** 345–3
[28] Zhang SS Xu K and Jow TR 2004 *Electrochim. Acta* **49** 1057–61
[29] Zhang SS Xu K and Jow TR 2006 *Electrochim. Acta* **51** 1636–40
[30] Liao L Zuo P Ma Y Chen X An Y Gao Y Yin G 2012 *Electrochim. Acta* **60** 269–73
[31] Li X Luo D Zhang X and Zhang Z 2015 *J. Power Sources* **291** 75–84
[32] Sharova V Moretti A Diemant T Varzi A Behm RJ Passerini S 2018 *J. Power Sources* **375** 43–52